Turkish Journal of Electrical Engineering & Computer Sciences

http://journals.tubitak.gov.tr/elektrik/

Research Article

Turk J Elec Eng & Comp Sci
(2013) 21: 1328 – 1339

doi:10.3906/elk-1111-65

A control algorithm for a simple flywheel energy storage system to be used in space applications

Kutlay AYDIN,[1] **Mehmet Timur AYDEMİR**[2,*]
[1]Turkish Aerospace Industries Inc., Kazan, Ankara, Turkey
[2]Department of Electrical and Electronic Engineering, Gazi University, Maltepe, Ankara, Turkey

Received: 30.11.2011 • **Accepted:** 11.03.2012 • **Published Online:** 12.08.2013 • **Printed:** 06.09.2013

Abstract: Flywheels have been under consideration to be used for energy storage purposes in space applications to replace electrochemical batteries. An electrical machine is used as a motor to store kinetic energy when the solar energy is available, and then the stored energy is converted back to electrical energy by running the machine as a generator when the solar energy is no longer available. A control algorithm for these systems is proposed in this paper. The proposed method uses a current reference rather than a speed reference in the motor mode. A method is also suggested to properly determine the current reference to overcome the losses and to create constant acceleration. The proposed algorithm is tested on an experimental set-up and the results are given.

Key words: Flywheel energy storage, motor-generator operation, satellite attitude systems

1. Introduction

Electrochemical batteries are the principal energy storage devices for satellites. However, the disadvantages of these batteries have led researchers to investigate alternatives such as flywheels. Flywheels are superior to electrochemical batteries in terms of their efficiency, depth of discharge, and lifetime. Furthermore, they do not have a negative impact on the environment like chemical batteries [1,2]. However, in spite of all of these advantages, there are some application difficulties concerning flywheels, which are also called mechanical batteries. The leading reason for this is the necessity of using higher technology and complicated methods in these systems. First of all, mechanical losses should be minimized, and therefore, low-loss bearings such as magnetic bearings or ceramic bearings are required. Moreover, a high-speed, high-efficiency electrical machine should be properly designed and produced [1,2].

A very important feature of flywheels in space applications is that they can be integrated with attitude control systems. In these systems, they can be used as angular momentum storage systems for attitude control and as mechanical batteries to store kinetic energy. This results in a smaller and lighter system, which is very advantageous for space applications.

Serious research has been conducted at the NASA Glenn Research Center in this area. Flywheel systems have been designed and produced in this center for the International Space Station. The flywheel was designed for 60,000 rpm, with a storage capacity of 364 Wh [1]. The mechanical losses of the system were minimized using active magnetic bearings for suspension. Moreover, a high-speed permanent magnet synchronous machine was designed and its field orientation control was realized. The design criteria and control methods for the

*Correspondence: aydemirmt@gazi.edu.tr

motor were reported in [3,4]. An optical sensor was utilized for the rotor position and speed measurements. In another work, 2 different methods for different operation speeds were proposed to drive the motor without this sensor [5]. Later, bus regulation circuitry for the discharge mode was added to the energy storage system [6,7], and, eventually, energy storage and attitude control functions were integrated. A single-axis attitude control was established, and attitude control along with energy storage was realized simultaneously [8,9].

Traditionally, induction motors are used in flywheel energy storage applications. However, there has been an interest in using permanent magnet machines for these applications. A permanent magnet DC machine and permanent magnet AC machine were coupled together to emulate the system in [10]. However, 2 separate controllers were used for the motoring and generating periods. These motors have also been suggested for use in different applications of flywheel energy storage systems. For example, a 3.6-MJ system was suggested for mobile transportation vehicles such as heavy trucks [11], and a 580-kJ system was suggested for pulsed power application [12]. At least in one case, axial flux permanent magnet machines were also proposed for flywheel energy storage systems [13].

Dynamic control of a permanent magnet synchronous motor-driven reaction wheel was reported in [14]. The control algorithm was adapted according to the variations of the friction and disturbances using the friction estimation of the system.

In this paper, a new control algorithm is proposed for flywheel energy storage systems that can be used in space applications. In the proposed method, a current reference is used to drive the machine in the motor mode. This is especially important to overcome the effects of the mechanical losses. The proposed algorithm is tested on an experimental set-up and the results show that the algorithm works.

In the following section, the general structure of the system is given. In Section 3, the proposed control algorithm is presented. The operation of the system in both modes is described in detail and a method to estimate the loss mechanisms is given. The experimental results are shown in Section 4. Finally, the conclusion and future work are given in Section 5.

2. Structure of the flywheel energy storage system

Since the energy storage capacity is proportional to the square of the rotational speed, high-speed machines such as permanent magnet machines are the natural choice for these systems. Therefore, a 2-pole, 50-W brushless DC (BLDC) motor was used in this work. The maximum speed of the motor at a rated voltage (32 V) is 38,000 rpm, and the maximum allowed speed is 50,000 rpm.

Figure 1 shows the drive and control structure used [15,16]. The block commutation technique was implemented. The position information of the rotor was sensed by the Hall-effect sensors integrated with the motor. A direct current reference was used to drive the motor. The speed feedback loop was used only for over-speed protection.

In the start-up of the system, a constant current reference is applied to the controller to drive the motor to a predetermined speed. The purpose is to bring the flywheel to the minimum operation speed. Since the torque is directly proportional to the current, control is achieved through the current amplitude. The current commutation block in Figure 1 is used for this purpose. The phase currents are measured using shunt resistors. In the current commutation block, the phase current values for phases a and b are measured, and phase c current is then calculated. Finally, the peak value of the phase currents (I_m) is obtained using these data. This DC current value is compared to the references and the resulting error is processed by a proportional-integral (PI) controller to obtain the voltage reference. This reference is the input for the voltage commutation block.

A symmetrical pulse-width modulation (PWM) switching signal is generated inside the voltage commutation block by comparing the voltage reference and the triangular carrier signal. MOSFETs are used as the switching devices, and the switching frequency is selected as 20 kHz. Hall sensor outputs that depend on the rotor position are used to determine which switches are turned on or off. The true speed information of the motor is also obtained from the Hall sensor signals.

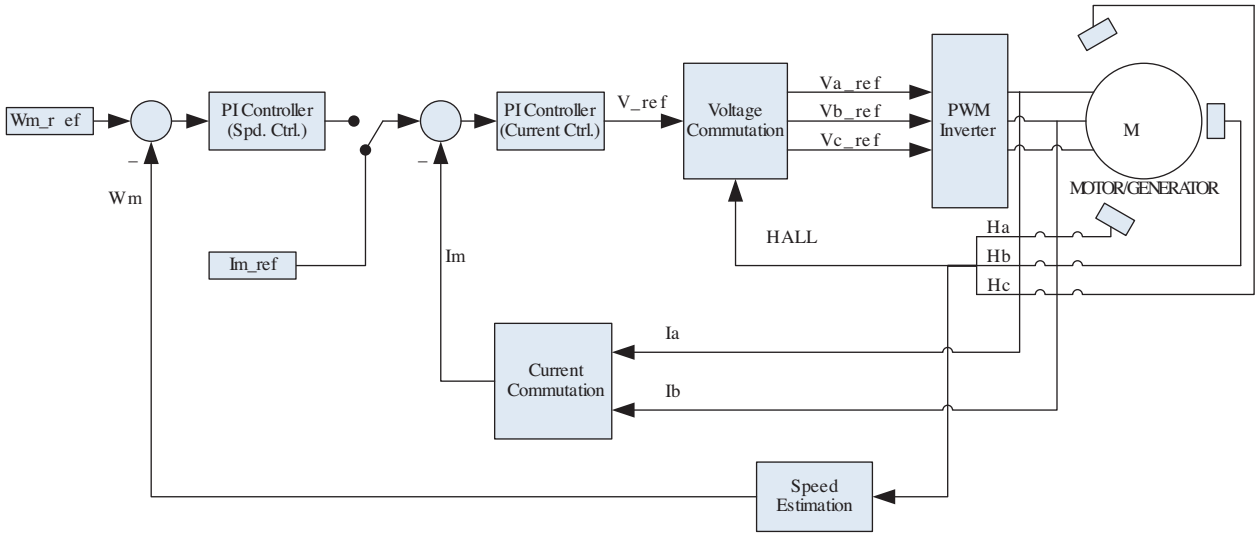

Figure 1. Drive and control structure.

The current reference that is used to drive the motor is defined as a function of speed since the torque components resulting from the bearing friction and windage also depend on the speed. Therefore, the torque developed by the motor and the motor current should be a function of the speed. Details on this are given in Section 3.

The phase inductance values of high-speed motors are typically low in microhenry levels. Therefore, the phase currents are discontinuous when PWM signals are used, resulting in various torque harmonics. External inductors are used in series with the phase windings to mitigate this effect. These inductors are also needed to use the inverter as the boost rectifier during the discharge mode.

3. Proposed control algorithm for the flywheel energy storage system

Separate flywheel controls are designed for 2 operation stages. These are the charging (motor) and discharging (generator) modes. During the charging mode, energy provided by the solar panels is enough to supply the motor and the other loads. The DC bus regulation in this mode is undertaken by the satellite power system. A threshold value is defined to determine the transition between the 2 modes. When the DC bus voltage drops below this threshold, it is decided that the solar power is not enough anymore and the electrical connection between the panels and the loads is removed. The discharge mode starts at this instant. In this mode, the loads are supplied by the BLDC machine that operates as a generator. The DC bus voltage regulation duty is now undertaken by the flywheel. Figure 2 shows a simple block diagram of the satellite power system and flywheel energy storage system.

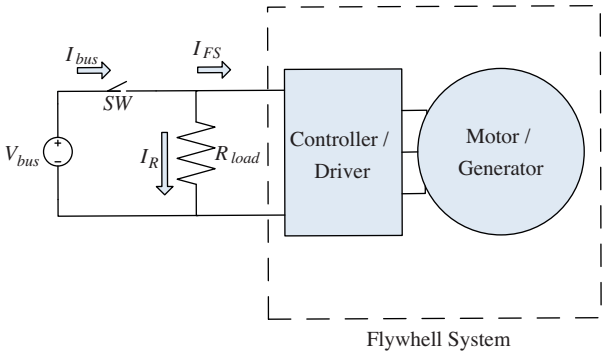

Figure 2. Block diagram of a satellite power system including a flywheel energy storage system.

The motor is driven by a current reference signal during the charging mode. A proper current reference is obtained using the power balance of the system:

$$E_m I_m = \tau_e \varpi_m = P_{out}, \tag{1}$$

where E_m is the peak value of the back electromotive force (EMF) voltage in V, I_m is the peak value of the phase current in A, τ_e is the electromechanical torque developed by the machine in N m, ω_m is the mechanical speed of the machine in rad/s, and P_{out} is the output power in W.

The electromechanical torque equation of the machine is given in Eq. (2):

$$\tau_e = J\frac{d\varpi_m}{dt} + B\varpi_m + \tau_L, \tag{2}$$

where J is the inertia of the flywheel in kg m^2, τ_L is the load torque in N m, and B is the friction coefficient in Nms.

Although it is shown in Eq. (2), the τ_L component is zero since there is actually no mechanical load in the flywheel system. Moreover, the windage losses will be zero since the system operates in a vacuum.

Using Eqs. (1) and (2), the peak value of the motor phase current is obtained. This value is used as the current reference in the flywheel control system.

$$I_m = \frac{(J\frac{d\varpi_m}{dt} + B\varpi_m)\varpi_m}{E_m} = \frac{P_{acc} + P_{fr}}{E_m} \tag{3}$$

Here, P_{acc} is the acceleration power in W and P_{fr} is the friction power loss in W.

In order to use Eq. (3), the friction coefficient needs to be calculated and the flywheel speed and motor back EMF need to be estimated. The control architecture of the system is shown in Figure 3.

3.1. Charging mode

In the charging mode, the flywheel is charged by a DC power supply representing the solar panels. The current reference given in Eq. (3) is used at this stage. The current control is designed to overcome the mechanical losses and to create constant acceleration. The current reference is variable since there are speed-dependent losses. Active sections of the flywheel system architecture during this stage are shown in Figure 4.

The system enters the charging mode when the SW switch on the DC bus is turned on when the bus voltage is over a predetermined level. Energy coming from solar panels is used to supply the load and to accelerate the motor at the same time. A DC power supply is used in the experiments instead of solar panels.

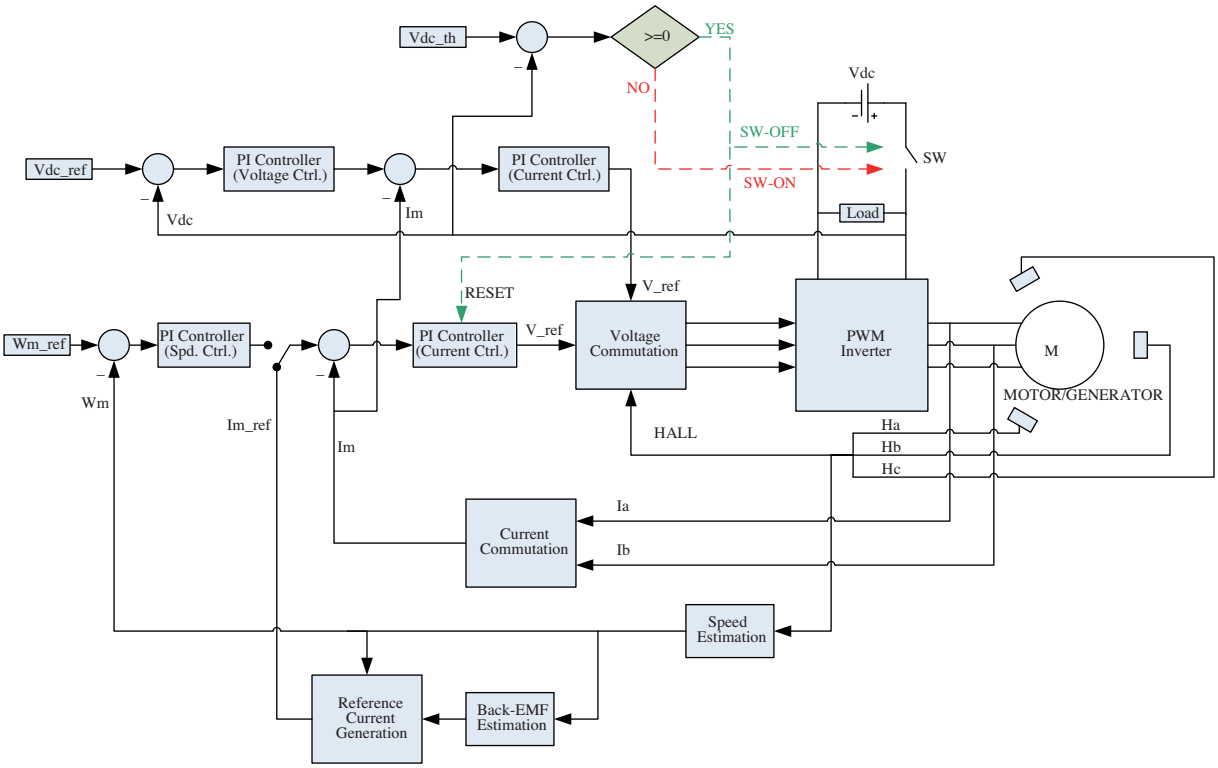

Figure 3. Flywheel control architecture.

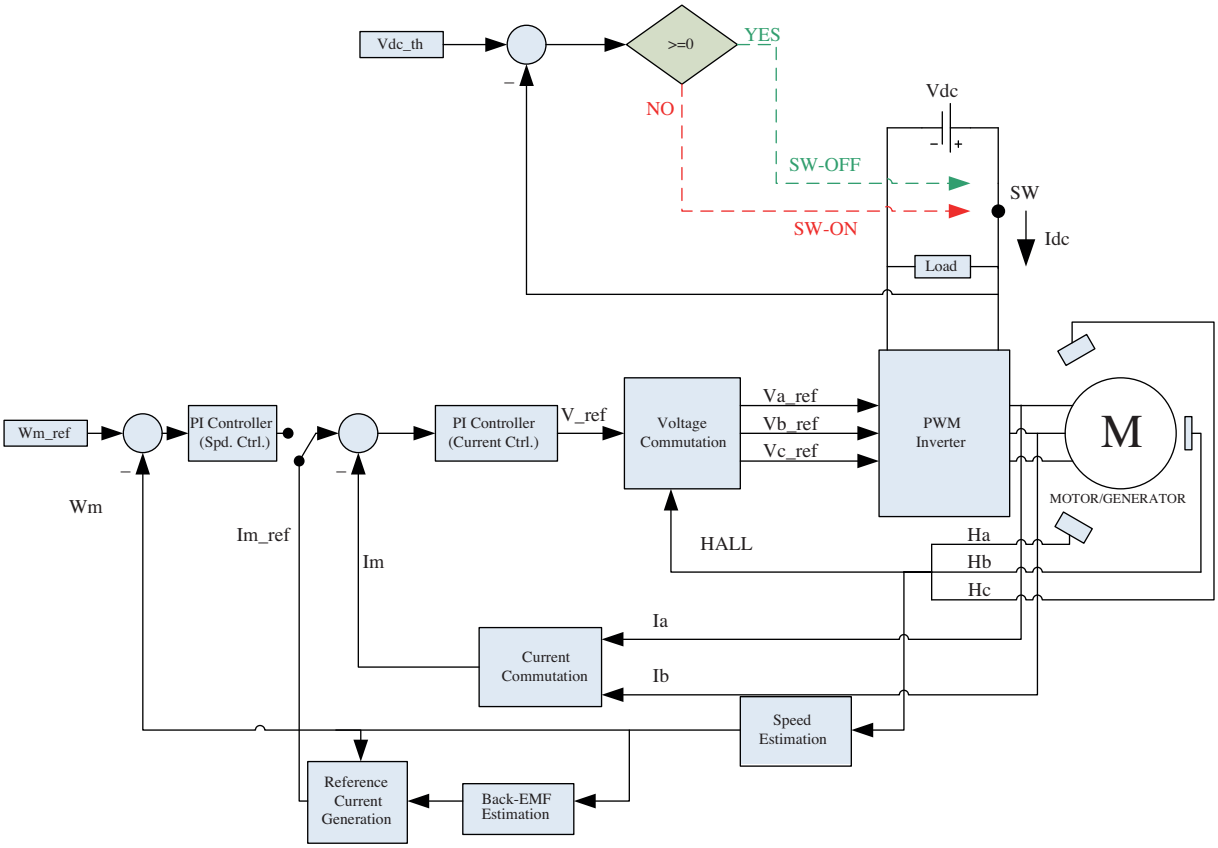

Figure 4. System during the charging (motor) mode.

A speed loop in the motor controller is used only for over-speed protection. When the speed reaches a predetermined speed limit, this loop is activated and the motor speed is regulated at this level. As long as the speed is below this limit, the motor is driven by the current reference that is defined in Eq. (3). The friction power loss has been calculated for the steel ball bearings and is included in the algorithm. The back EMF constant (K_V) of the BLDC machine is used to calculate the peak value of the back EMF voltage.

$$E_m = \varpi_m / K_V \tag{4}$$

Hall sensor pulses are used to calculate the speed. The output of a counter that is activated at the half-period of each Hall sensor pulse is used for this purpose.

The current commutation block computes a phase C current using phase A and phase B current measurements. Next, a DC control current (I_m) is obtained using the peak values of these currents.

The current controller is a PI regulator, and the voltage reference is obtained at its output. This voltage reference is multiplied by the Hall-effect sensor signals in the voltage commutation block to obtain the voltage references for each phase. These phase voltage references are compared to 20-kHz triangular carrier signals to generate the PWM switching signals.

3.2. Discharge mode

When the solar energy is no longer sufficient, the DC bus voltage drops below the predefined threshold level and the SW switch is turned off by the controller, initiating the discharge mode. The load, which is just a resistor here, is supplied by the generator. The active sections of the system in this mode are shown in Figure 5.

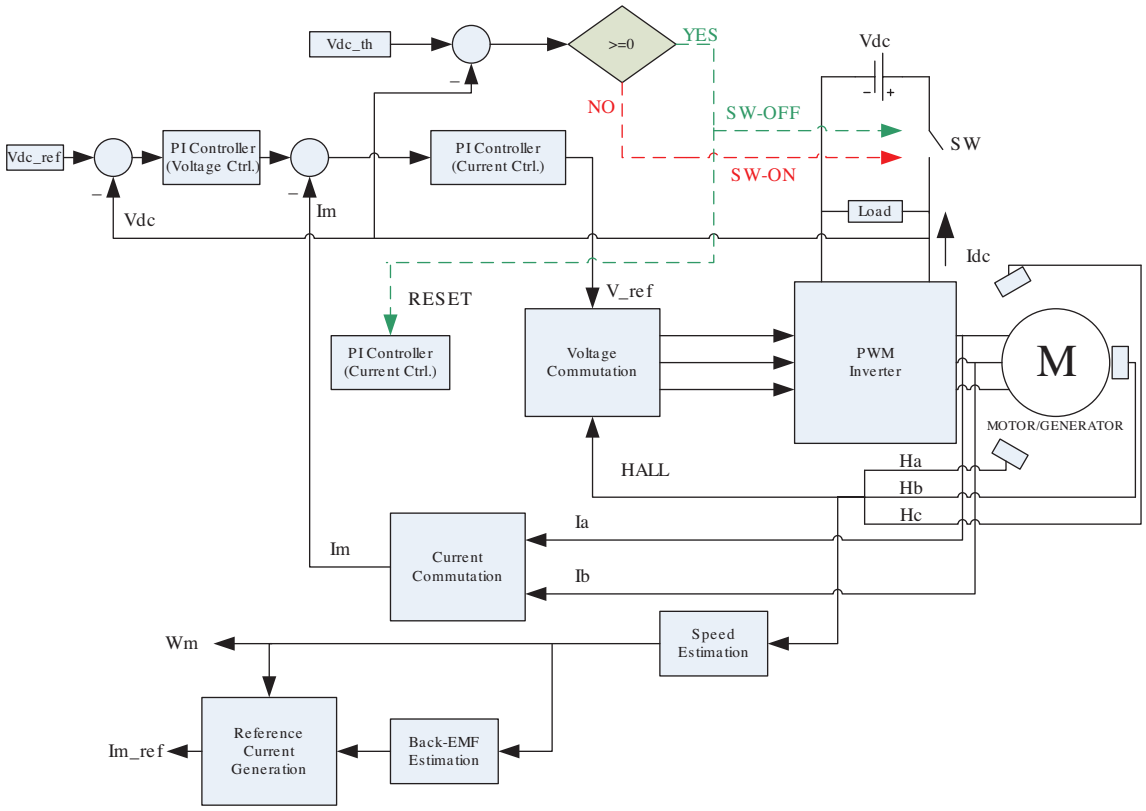

Figure 5. System during the discharge (generator) mode.

The DC bus voltage is regulated at a predetermined level in this mode. The PWM inverter is used as a PWM boost rectifier in this mode for this purpose. The DC bus voltage is first compared to the reference voltage to generate a current reference that is then compared to the real current (I_m). A different control algorithm, the boost algorithm, is used inside the voltage commutation block in this mode. The phase voltage reference signals are obtained by the boost algorithm, and these signals are compared to the 20-kHz triangular carrier signals to generate the PWM switching signals.

The current reference and speed estimate algorithms continue to run during the discharge mode since their outputs should be available when the next charging mode starts.

The accumulated output of the integrator may cause the voltage references to reach very high values in the generator mode. This, in turn, may result in very high instantaneous motor currents, leading to the activation of the over-current control during the transition from the generator mode to the motor mode. The current controller needs to be reset before initiating the generator mode to prevent this problem.

4. Experimental results

The experimental set-up seen in Figure 6 was used to test the system. A DC power supply was used instead of solar panels, and the switch on the DC bus was controlled manually. A Maxon EC22 BLDC was used as the motor/generator unit. A Technosoft MCK2812 was chosen as the flywheel driver. The control algorithm was developed in a DMC28x Developer Pro software environment. A 500-μH external inductor was placed in series with the phase windings to reduce the current ripple and for the boost operation in the generator mode.

Figure 6. Experimental set-up.

It should be noted that these systems are normally designed for space applications and, therefore, either magnetic or ceramic bearings are used to minimize the mechanical losses. There are no windage losses either, since the system operates in a vacuum. However, the experimental set-up is not operated in a vacuum, and standard steel ball bearings are used. Therefore, the losses are high. As a result, the speed is limited to 9500 rpm and the stored energy is not very high. The charging and discharging intervals have been kept short to demonstrate the concept. For the same purpose, high-resistance loads (5 kΩ and 310 Ω) have been used to prevent fast speed reductions.

In light of this information, Eq. (3) needs to be modified if the power loss due to the windage effects (P_{wnd}) is added.

$$I_m = \frac{P_{acc} + P_{fr} + P_{wnd}}{E_m} \tag{5}$$

Power loss due to windage and mechanical friction is usually defined by empirical equations. The following equations have been used in this work [17]. The shaft diameter has been ignored in the calculations of the windage losses.

$$P_{fr} = \frac{1}{2} * \varpi_m * K_{fr} * F * D_b watt \tag{6}$$

$$P_{wnd} = \frac{1}{64} * C_M * \rho * \varpi_m^3 * D_r^5 watt \tag{7}$$

Here, K_{fr} is the friction coefficient (0.001–0.005), F is the force acting on the bearings (N), D_b is the inner diameter of the bearing (m), ω_m is the flywheel angular speed (rad/s), C_M is the torque constant, $\rho$is the density of the air (kg/m^3), and D_r is the flywheel diameter (m).

The Reynold number needs to be determined first to calculate the torque constant:

$$R_e = \frac{\rho \varpi_m D_r^2}{4\mu}. \tag{8}$$

The variable μ in this equation represents the dynamic viscosity and it is 1.8 10^{-5} kg/m s for 1 atm at 20 °C. The air density is 1.2 kg/m^3 for the same conditions. A flywheel with a diameter of 0.135 m is used. If the Reynold number is calculated for the flywheel speeds below 10,000 rpm (1047 rad/s) it is found to be less than 230,776. In this case, the torque constant can be calculated as follows [12]:

$$C_M = \frac{3.870}{R_e^{0.5}}. \tag{9}$$

In order to determine the losses caused by the bearing, the friction forces acting on the bearings need to be known. In the system under consideration, these forces are the force due to the flywheel weight (F_G) and the imbalance forces (F_B).

$$F = F_G + F_B \tag{10}$$

The imbalance force can be calculated as follows:

$$F_B = me\varpi_m^2, \tag{11}$$

where m is the residual mass (kg), e is the eccentricity between the rotational axis of the flywheel and the center of gravity (m), and me is the residual unbalance (kg m).

The total force acting on the flywheel is then:

$$F = F_G + F_B = Mg + me\varpi_m^2, \tag{12}$$

where g is the gravity (10 m/s^2) and M is the flywheel mass (0.233 kg).

The manufacturer of the bearings defines the friction coefficient (K_{fr}) as approximately 0.003. The only unknown left then is the residual unbalance (me). This value can be determined experimentally. The motor is accelerated to a certain speed by the constant current reference. Afterwards, the acceleration power is zero ($P_{acc} = 0$) and the motor is driven by the current reference that is calculated using the windage and friction loss values. It is expected that the motor will keep the final speed reached by the constant current reference if

the reference value is calculated correctly. A residual unbalance value of 1175 g mm has met this condition for the experimental set-up.

The acceleration power defined in Eq. (3) is written in a different way in Eq. (13).

$$P_{acc} = (J\frac{d\varpi_m}{dt})\varpi_m watt \tag{13}$$

The parameters used in the power equations are finally obtained as follows:

$K_{fr} = 0.003$

$F = (0.235\ 10 + 1.175\ 10^{-3}\omega_m^2)$ N

$D_r = 0.135$ m

$D_b = 0.010$ m

$J = 4.8 \times 10^{-4}$ kg m^2

$d\omega_m =$ 30,000 RPM (3141.6 rad/s)

$dt = (65 \times 60)$ s

As a result, aside from the acceleration power, the friction and windage losses can be defined as a function of the flywheel speed:

$$\begin{aligned} P_{acc} &= 3.870e^{-4}\varpi_m \\ P_{fr} &= (2.35 + 1.175\mathrm{e}^{-3}\varpi_m^2) * \varpi_m \\ P_{wnd} &= 18.67e^{-8}\frac{\varpi_m^3}{\varpi_m^{0.5}} \end{aligned} \quad . \tag{14}$$

In the experiments, the motor has been driven by a constant current reference of 386 mA (I_m_ref) for 60 s. Next, the calculated reference value has been used to drive the motor at a constant speed ($P_{acc} = 0$). The result is given in Figure 7.

In the second stage, the P_{acc} given in Eq. (14) is applied at t = 60 s and an acceleration test is conducted. The results are given in Figure 8. The expected acceleration is 7.7 rpm/s. The acceleration is calculated as 8 rpm/s from the test results given in Figure 8. The error is caused by the difficulty of calculating the real values of the friction and windage losses.

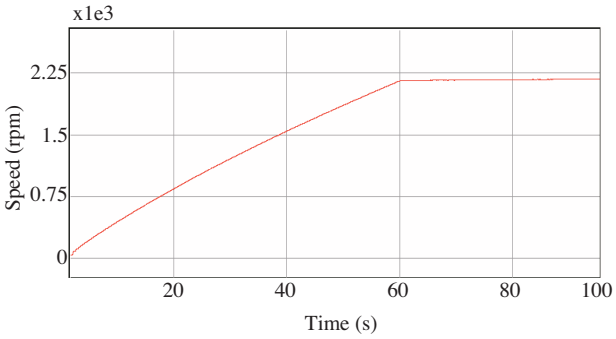

Figure 7. Result of the test to calculate the friction coefficient experimentally by driving the motor with a calculated current reference.

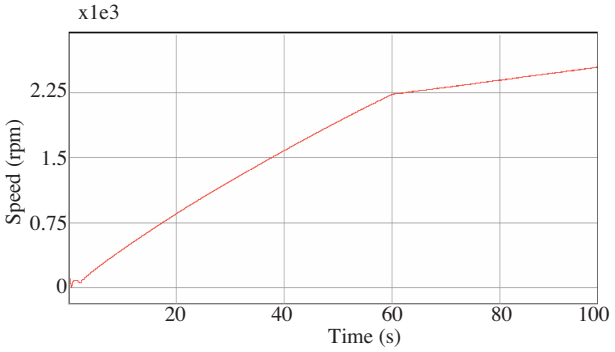

Figure 8. Constant acceleration operation profile of the flywheel.

Once the necessary adjustments are done, subsequent motor-generator operation tests can be performed. In the motor operation, a high value of acceleration of 143 rpm/s (15 rad/s^2) is used to drive the motor to the

maximum speed (9500 rpm) in a short time (75 s). At this instant, the 32-V bus voltage is disconnected and the generator mode is initiated. In the generator mode, first a 5 kΩ resistance was used as the load. In this mode, the bus regulation is performed by the flywheel system and it was designed to regulate the voltage at 13.9 V. This value was chosen due to the practical limitations arising from the low back EMF voltage value of the available motor (around a 7.8-V peak) at this speed. The speed variation in the generator mode is given in Figure 9 and the bus voltage variation is shown in Figure 10.

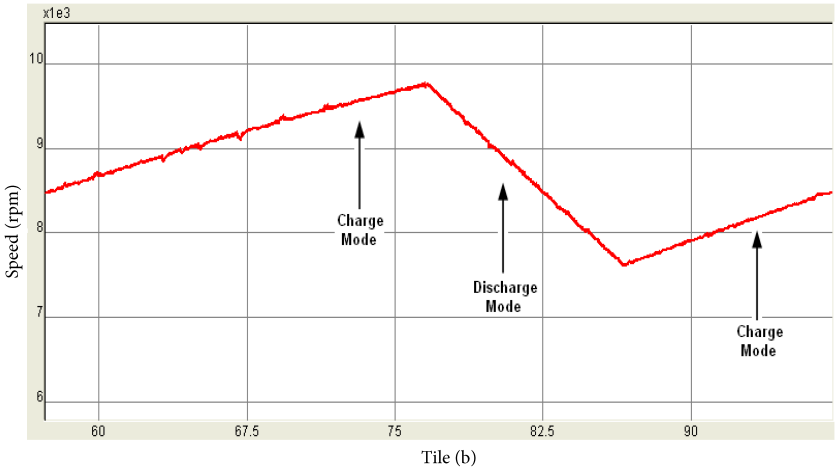

Figure 9. Flywheel speed variation during the generator's operation (load resistance is 5 kΩ).

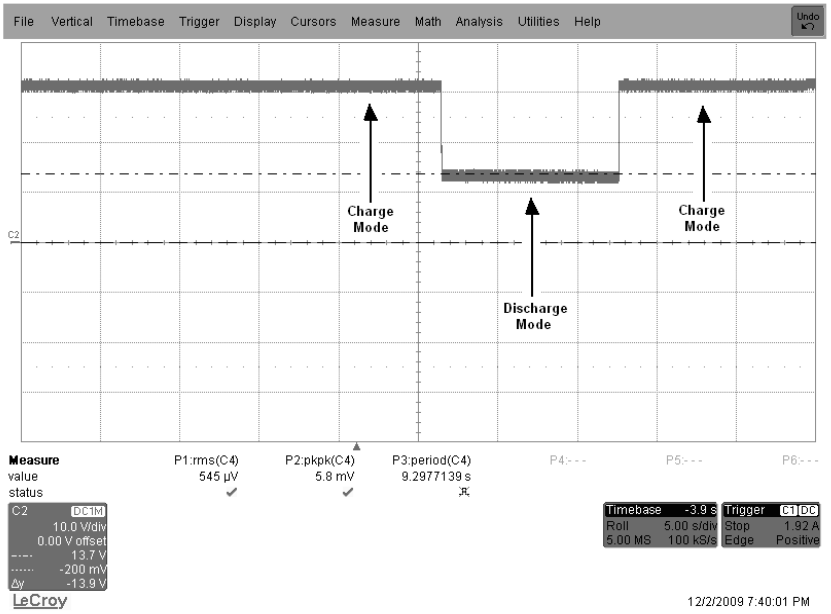

Figure 10. Bus voltage variation during the generator's operation (load resistance is 5 kΩ).

As seen from Figure 10, the bus voltage can be regulated at 13.7 V. Following the generator mode, 32 V of bus voltage is reapplied and the motor starts acceleration again as expected.

The operation stability at varying load conditions in the generator mode is also an important performance parameter. To test the system for this concept, the load was changed from 5 kΩ to 310 Ω and then back to 5

kΩ during operation. The speed and bus voltage variations for this operation are given in Figures 11 and 12, respectively.

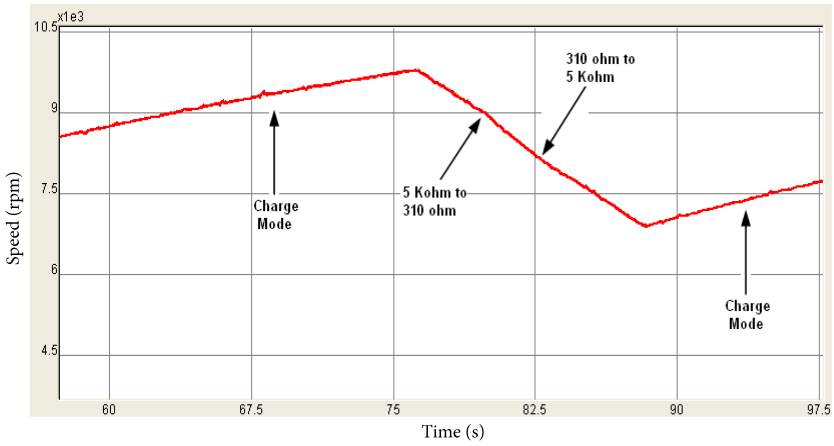

Figure 11. Flywheel speed variation during the generator's operation (load resistance is changed from 310 Ω to 5 kΩ).

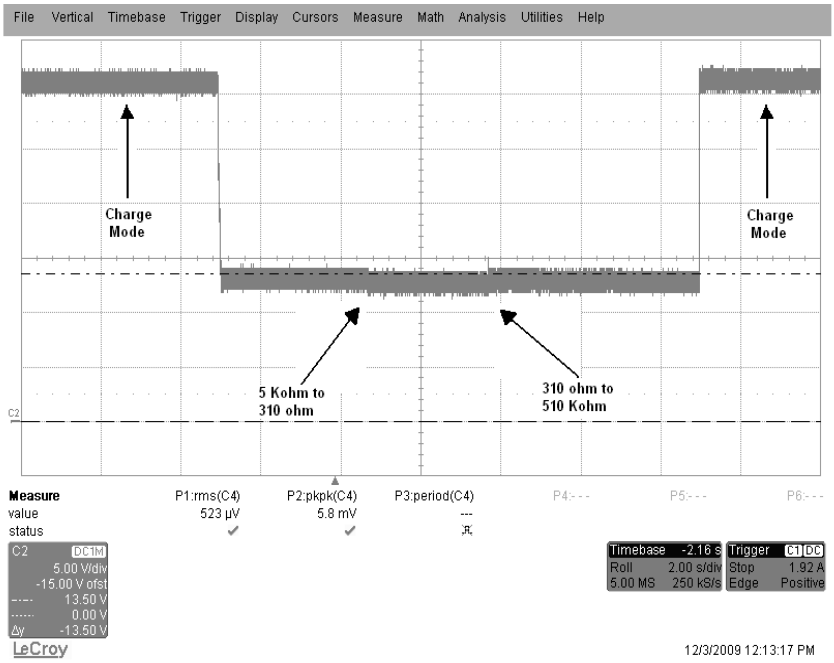

Figure 12. Bus voltage variation during the generator's operation (load resistance is changed from 310 Ω to 5 kΩ).

In this operation, the generator mode is started with 5 kΩ. About 4 s later, the load is changed to 310 Ω. After 3 s of operation at this condition, the load is brought back to 5 kΩ. As seen in Figure 12, the bus regulation is not dramatically affected by this load variation.

5. Conclusion

A simple flywheel energy storage system for space applications was investigated in this paper. A control algorithm was presented and the experimental results were given. The current reference instead of the speed reference was proposed to drive the machine in the charging mode to avoid instantaneous current variations.

This requires a good estimation of the mechanical losses, and a method was proposed for this purpose. A bus voltage regulation algorithm was successfully applied during the generator (discharging) mode. The transition between the operation modes was realized without any problems. Due to the physical limitations, the operation speed was limited to below 9500 rpm.

The application of the algorithm presented in this paper to flywheel systems with magnetic and ceramic bearings is planned. This will provide a good chance to compare the results. Moreover, the effects of the energy storage function on the attitude control may be investigated if this system is utilized in an integrated power and attitude control system for spacecrafts.

References

[1] B.H. Kenny, P.E. Kascak, R. Jansen, T.P. Dever, W. Santiago, "Control of a high-speed flywheel system for energy storage in space applications", IEEE Transactions on Industry Applications, Vol. 41, pp. 1029–1038, 2005.

[2] M.R. Patel, Spacecraft Power Systems, CRC Press, Boca Raton, FL, USA, 2005.

[3] B.H. Kenny, P.E. Kascak, H. Hofmann, M. Mackin, W. Santiago, R. Jansen, "Advanced motor control test facility for NASA GRC flywheel energy storage system technology development unit", 36th Intersociety Energy Conversion Engineering Conference, 2001.

[4] A.S. Nagorny, N.V. Dravid, R.H. Jansen, B.H. Kenny, "Design aspects of a high speed permanent magnet synchronous motor/generator for flywheel applications", IEEE International Conference on Electric Machines and Drives, pp. 635–641, 2005.

[5] B.H. Kenny, P.E. Kascak, "Sensorless control of permanent magnet machine for NASA flywheel technology development", NASA TM 2002-211726, 2002.

[6] P.E. Kascak, B.H. Kenny, T.P. Dever, W. Santiago, R.H. Jansen, "International space station bus regulation with NASA GRC flywheel energy storage system development unit", NASA TM 2001-211138, 36th Intersociety Energy Conversion Engineering Conference, 2001.

[7] B.H. Kenny, P.E. Kascak, "DC bus regulation with a flywheel energy storage system", SAE Power Systems Conference, 2002.

[8] P.E. Kascak, R.H. Jansen, B.H. Kenny, T.P. Dever, "Single axis attitude control and DC bus regulation with two flywheels", 37th Intersociety Energy Conversion Engineering Conference, pp. 214–221, 2002.

[9] B.H. Kenny, R.H. Jansen, P.E. Kascak, T.P. Dever, W. Santiago, "Demonstration of single axis combined attitude control and energy storage using two flywheels", Proceedings of the IEEE Aerospace Conference, Vol. 4, pp. 2801–2819, 2004.

[10] B. Vafakhah, M. Masiala, J. Salmon, A. Knight, "Emulation of flywheel energy storage systems with a PMDC machine", 18th International Conference on Electrical Machines, pp. 1–6, 2008.

[11] A.M. Knight, J. Salmon, H. Syed, B. Vafakhah, J. Ewanchuk, "A compact variable speed drive for mobile flywheel energy storage systems", International Conference on Electrical Machines, pp. 1–6, 2010.

[12] S. Talebi, B. Nikbakhtian, A.K. Chakali, H.A. Toliyat, "Control design of an advanced high-speed FESS for pulsed power applications", 34th Annual Conference of the IEEE Industrial Electronics, pp. 3358–3363, 2008.

[13] T.D. Nguyen, K.J. Tseng, C. Zhang, S. Zhang, H.T. Nguyen, "Position sensorless control of a novel flywheel energy storage system", IPEC Conference Proceedings, pp. 1192–1198, 2010.

[14] M.G. Chou, C.M. Liaw, "Dynamic control and diagnostic friction estimation for an SPMSM-driven satellite reaction wheel", IEEE Transactions on Industrial Electronics, Vol. 58, pp. 4693–4707, 2011.

[15] R. Krishnan, Electric Motor Drives, Prentice Hall, Hoboken, NJ, USA, 2001.

[16] MCK2812 User Manual, available at http://www.technosoftmotion.com/products/Freedemo-tools.php.

[17] J. Pyrhönen, T. Jokinen, V. Hrabovcova, Design of Rotating Electrical Machines, Wiley, New York, 2008.